Diffraction-ray optics of laser-pulse filamentation

Yu. E. Geints* and A. A. Zemlyanov
V. E. Zuev Institute of Atmospheric Optics SB RAS, Zuev Square 1, 634021 Tomsk, Russia

(Received 12 January 2018; published 23 August 2018)

We present a qualitative description of the laser-pulse filamentation phenomenon based on light field representation as a self-consistent ensemble of specific localized wave structures known as the diffraction-ray (light) tubes. These light tubes are energetically independent from each other and, at the same time, they are in close field interaction through the phase front of the light wave. The trajectories of light tube centroids represent the evolutionary line of the Poynting vector transverse component. Light tubes do not intersect in space although they can be nested, and the tubes do not exchange light energy with each other. Spatial shape and area of light tubes can vary during pulse propagation, reflecting the influence of different physical processes manifesting themselves upon radiation propagation in a medium. This diffraction-ray approach applies the attributes of the amplitude and phase analysis to the problem of laser radiation self-action and sheds light on the onset and termination conditions of laser-pulse filamentation.

DOI: 10.1103/PhysRevA.98.023846

I. INTRODUCTION

The propagation of high-power ultrashort laser pulses in transparent media is realized predominantly in the nonlinear regime and is characterized by a large-scale spatiotemporal phase and amplitude modulations of the light field. In optical media with a strong cubic nonlinearity (Kerr-type nonlinearity), a high-intensity light pulse undergoes self-focusing which results in sharp compression of pulse spatial dimensions and avalanche intensity increase. Pulse transverse collapse is arrested by the multiphoton absorption and plasma generation in a medium at high field intensities ($>10^{13}\,\mathrm{W/cm^2}$), as well as by the processes associated with the higher-order optical nonlinearities (HOKE). Such multifactorial interplay of different physical factors results in the formation of pulse nonlinear focus after which a narrow high-intensity light filament or group of filaments is formed in the propagation direction [1]. The angular divergence of this filament is less than the diffraction-limited divergence of the entire beam in a linear medium.

In experiments on the filamentation of femtosecond radiation, the trace of filaments is registered as luminous channels in the visible region, which are formed in the course of free-electron recombination with neutrals and ions. In air and other transparent media (water, glass), the peak intensity in the filament can reach tens of $\mathrm{TW/cm^2}$, while mean filament dimensions vary by hundreds of micrometers depending on the type of propagation medium and laser wavelength [1]. High intensity in the filaments causes medium ionization and initiates plasma production with a characteristic free-electron density of about $10^{15}-10^{18}\,\mathrm{cm^{-3}}$ [2], which in particular forces medium luminescence. There are many scientific works devoted to various aspects of laser-pulse self-focusing and filamentation in air. The current state of the problem of laser-pulse filamentation is presented, e.g., in several comprehensive reviews [1,3,4].

With the advent of high-power femtosecond lasers in research practice, the phenomenon of laser filamentation has acquired great importance for various areas of nonlinear optics and laser physics. These include laser technology aspects, e.g., femtosecond nanostructuring and micromachining of various media, generation of ultra-broad-band (supercontinual) optical radiation [5–7], as well as atmospheric-optical applications related to terrestrial electricity, remote environmental laser diagnostics, and directional long-range transmission of high-power laser radiation [8–11].

Theoretical studies of high-power femtosecond pulse filamentation in various physical media with a wide variation of laser radiation parameters and geometrical setups have been the subject of many scientific papers, estimated to date to be in the thousands. For physical interpretation of pulse filamentation and building a qualitative picture of this phenomenon, several theoretical models were proposed in the literature, all based on numerical simulations and available experimental data. The most popular physical models are (a) the treatment of a filament as a self-induced refractive waveguide in a medium [12,13], (b) the filament as a sequence of moving nonlinear (dynamic) foci [14,15], and (c) the model of a spatial optical quasisoliton [16], which dynamically replenishes its energy from the surrounding "energy reservoir" of the peripheral beam areas [7,17]. Each physical model initially was based on a certain set of experimental information, and therefore describes only specific aspects of the filamentation process.

As a rule, the physics of filamentation is studied by analyzing the amplitude characteristics of the measured quantities, e.g., optical field intensity, energy density (fluence), electrical conductivity of the filamented core, spectral density of laser plasma luminescence, and acoustic pressure. Therefore, all above-mentioned filamentation models as inputs use the physical parameters expressed also in the form of amplitude or energy values. At the same time, the phase of an optical wave is as informative as its amplitude because it also contains the imprints of all linear and nonlinear processes that occur with the radiation as it propagates in the medium. Also, it is

*Corresponding author: ygeints@iao.ru

the local slope of the phase front that determines the direction of power and energy fluxes within the light wave [18].

A striking example of combined amplitude-phase treatment of laser radiation self-action is the technique of optical ray tracing which constructs ray patterns for a laser beam propagating in a nonlinear medium [18–22]. These ray pictures represent a family of geometric or diffraction-geometric (diffraction) rays [23] the trajectories of which obey evolutionary laws governed by the fundamental pulse propagation equation [24]. Every diffraction ray (DR) represents an integral trajectory coinciding with the streamline of the Poynting vector. A finite number of closely spaced diffraction rays form a localized light structure, known as a light (diffractive-ray) tube (DRT) [25,26].

Unlike an infinitely thin ray, a light tube is characterized by a finite cross section and carries a certain amount of radiation power (energy). The fundamental property of a DRT is the constancy of the energy flowing through any of its cross sections, if there are no sources and sinks of energy in the medium. The main reason for using the DRT methodology is that the spatial evolution of light wave amplitude in a medium can be represented as a picture of DRTs each carrying a certain portion of light energy. In photometry, such a formal replacement is a powerful tool in analyzing the spatial distribution of illumination in a complex scene configuration [26]. In optics of femtosecond pulses, a similar analysis was successfully applied in studying the regularities of filamentation in unimodal beams with different profiles [21,22,27], and also the evolution of radiation at the postfilamentation stage of pulse propagation [28].

Worth noting, the ray-tracing methodology for the visualization of the electromagnetic vectorial field inherits the Bohmian formulation of quantum mechanics [29] as applied to the photons [30,31]. Analogous ray-based treatment can be found in different scientific areas, e.g., in quantum chemistry for molecular magnetic currents [32] or even for sound wave energy streamline rendering [33].

In this paper, we further develop the theoretical concept of the light field as an ordered collection of spatially localized wave structures that are energetically independent from each other and simultaneously located in close interaction through the wave phase front (diffraction). As a visualizing tool of these light structures and interpretation of the information contained in the optical phase, the mathematical formalism of the diffraction-ray tubes is proposed. Although the light ray representation of laser-pulse filamentation was known earlier [21–28], here we give a comprehensive mathematical justification for this technique. The classical definition of a light tube derived for the stationary field is extended to the case of nonstationary light field propagation in a nonlinear dissipative medium with chromatic dispersion (of the second order). As an example, we construct DRT patterns for analyzing the dynamics of nonlinear propagation of high-power ultrashort laser pulses in the self-focusing and filamentation regimes in air. In particular, the proposed diffraction-ray tube formalism allows us to precisely localize and trace the evolution of the specific spatial region of the laser pulse, called in the literature the "energy reservoir" [17], which provides light energy for filament existence. With DRT tracing it becomes possible to reveal the actual role of this energy reservoir in filament formation. Also, DRT pictures help in evaluating the energy refueling effect on the plasma-free postfilament propagation of a light pulse.

We emphasize that the diffraction rays and the light tubes are to a greater extent other optical tools for light propagation visualization, which extends the traditional wave "amplitude" analysis by the streamline picture of energy fluxes inside a propagating light pulse.

The paper is organized as follows. In Sec. II we provide for the complete mathematical formalism of the diffraction-ray optics in the laser-pulse filamentation problem. Here, we derive the evolutional equations for spatial and temporal diffraction rays and reveal the conservation laws in the light tubes. In Sec. III, several examples of diffraction-ray pictures of a classical Gaussian laser-pulse filamentation in air are presented. For this purpose, we directly solve the wave propagation equation [Eq. (1)] by the use-proven spectral method [1–3], obtain the complex-valued optical field, and then use it for the calculations of the wave phase and/or amplitude profiles on the propagation range. Having this information we use it for the derivation of the diffraction-ray trajectories. The diffraction-ray concept is extended to the light tube formalism in Sec. IV. The light tubes demarcate light energy fluxes within the beam so that each of them can be treated as a separate sub-beam with its own transverse dimensions and angular divergence. We introduce the averaged (effective) diffraction rays which represent the whole light tube as a single dimensionless trajectory, and in Sec. V we demonstrate how this methodology can be applied in studying the laser radiation filamentation dynamics especially on the postfilamentation evolutional stage.

II. DIFFRACTION-RAY MATHEMATICAL FORMALISM OF LASER-PULSE NONLINEAR PROPAGATION

As the basis for derivation of the diffraction-ray optics equations we take the paraxial wave equation for the complex amplitude of the electric field $E(\mathbf{r}_\perp, z\,; t)$ expressed in the coordinate system moving with pulse group velocity:

$$\frac{\partial E(\mathbf{r}_\perp, z\,; t)}{\partial z} = \frac{i}{2k_0}\nabla_\perp^2 E - i\frac{k_\omega''}{2}\frac{\partial^2 E}{\partial t^2} + \frac{1}{2}ik_0\frac{\varepsilon_N(\mathbf{r}_\perp, z\,; t)}{\varepsilon_0}E - \frac{1}{2}\alpha_N(\mathbf{r}_\perp, z; t)E. \tag{1}$$

Here, $k_0 = n_0\omega_0/c$ is the wave number, n_0 stands for the linear refractive index, ω_0 is the pulse central frequency, and k_ω'' is the second-order pulse group velocity dispersion (GVD). The nonlinear additive ε_N to linear medium dielectric permittivity ε_0 and the nonlinear absorption coefficient α_N account for potentially time-dependent cubic optical nonlinearity $n_2(t)$ (self-focusing), higher-order Kerr nonlinearities n_j , $j > 2$(HOKE), multiphoton light absorption, and plasma nonlinearity; the latter causes wave refraction and light absorption by the free-electron gas. The expressions for these quantities are as follows:

$$\varepsilon_N = 2n_0\sum_{j=2}^{J} n_j(t)|E|^{2(j-1)} - \frac{\sigma\omega_0\tau_c}{k_0}\rho_e, \tag{2a}$$

$$\alpha_N = \sigma\rho_e + \frac{W_I\Delta E_i}{|E|^2}(\rho_{nt} - \rho_e) \tag{2b}$$

with σ, τ_c, and ΔE_i denoting the inverse Bremsstrahlung cross section, electron mean collision time, and ionization potential, respectively. W_I is the photoionization rate of the medium with the density of neutral atoms (molecules) ρ_{nt}.

In the following, we use the amplitude-phase representation of the complex field by introducing the real amplitude $A(\mathbf{r}_\perp, z; t)$ and real-valued phase $\varphi(\mathbf{r}_\perp, z; t)$: $E = Ae^{i\varphi}$. After substituting this ansatz into Eq. (1) and collecting the real and imaginary parts we obtain two equations for the amplitude and phase of the wave:

$$\frac{\partial A}{\partial z} = -\frac{1}{2k_0}[A\nabla_\perp^2\varphi + 2(\nabla_\perp\varphi)\cdot(\nabla_\perp A)] + k_\omega''\left[\frac{\partial\varphi}{\partial t}\frac{\partial A}{\partial t} + \frac{1}{2}A\frac{\partial^2\varphi}{\partial t^2}\right] - \frac{\alpha_N}{2}A, \tag{3a}$$

$$\frac{2}{k_0}\frac{\partial\varphi}{\partial z} + \frac{1}{k_0^2}(\nabla_\perp\varphi)^2 - \frac{k_\omega''}{k_0}\left(\frac{\partial\varphi}{\partial t}\right)^2 = \frac{\varepsilon_N}{\varepsilon_0} + \frac{\nabla_\perp^2 A}{k_0^2 A} - \frac{k_\omega''}{k_0 A}\frac{\partial^2 A}{\partial t^2}. \tag{3b}$$

A. Diffraction rays

Let us turn to the equation for the wave phase, Eq. (3b), and for convenience introduce several notations on the right-hand side of this equation. Thus, $\varepsilon_d = \varepsilon_0\nabla_\perp^2 A/(k_0^2 A)$ is treated as the field diffractive component of medium dielectric permittivity, while $\varepsilon_{\rm dis} = -\varepsilon_0(\partial^2 A/\partial t^2)k_\omega''/(k_0 A)$ represents the dispersive-refractive part. Actually, the right-hand side of Eq. (3b) has the physical meaning of some effective dielectric permittivity of the medium, $\varepsilon_{\rm ef} = \varepsilon_0 + \varepsilon_N + \varepsilon_d + \varepsilon_{\rm dis}$, which accounts for, in addition to material dielectric permittivity ε_0, the field components originating from the nonlinearity of the medium ε_N, diffraction ε_d, and GVD $\varepsilon_{\rm dis}$ of the wave packet.

Next, we apply the transverse gradient operation ($\nabla_\perp$) to the left and right sides of Eq. (3b) and introduce a vector $\mathbf{s}_\perp = 1/k_0(\nabla_\perp\varphi)$ that represents the energy density flux through the lateral surface of a unit medium volume. This vector is directly related to the normalized transverse component of the Poynting vector $\mathbf{S}_\perp$ [18]: $\mathbf{s}_\perp = \mathbf{S}_\perp/A^2$. As a result, for this vector one obtains the following equation:

$$\frac{\partial\mathbf{s}_\perp}{\partial z} + (\mathbf{s}_\perp\cdot\nabla_\perp)\mathbf{s}_\perp - \left[k_\omega''\frac{\partial\varphi}{\partial t}\right]\frac{\partial\mathbf{s}_\perp}{\partial t} = \frac{1}{2}\nabla_\perp\bar{\varepsilon}_{\rm ef}, \tag{4}$$

where $\bar{\varepsilon}_{\rm ef} = \varepsilon_{\rm ef}/\varepsilon_0 - 1$.

Now, we apply the method of characteristics to Eq. (4) and rewrite it through the system of the Lagrange-Charpit ordinary differential equations [34] relative to the $\mathbf{s}_\perp$ vector:

$$\frac{dz}{dz'} = 1,\ \frac{d\mathbf{R}_d}{dz'} = \mathbf{s}_\perp,\ \frac{d\tau_{\rm dis}}{dz'} = -k_\omega''\frac{\partial\varphi}{\partial t},\ \frac{d\mathbf{s}_\perp}{dz'} = \frac{1}{2}\nabla_\perp\bar{\varepsilon}_{\rm ef}. \tag{5}$$

By introducing the variables $\mathbf{R}_d$, z, and $\tau_{\rm dis}$ we come to the characteristic equations for the spatial and temporal coordinates of the DR:

$$\frac{d\mathbf{R}_d}{dz} = \mathbf{s}_\perp = \frac{1}{k_0}\nabla_\perp\varphi(\mathbf{R}_d, z; \tau_{\rm dis}), \tag{6a}$$

$$\frac{d\tau_{\rm dis}}{dz} = -k_\omega''\frac{\partial\varphi(\mathbf{R}_d, z; \tau_{\rm dis})}{\partial t}. \tag{6b}$$

The DR's trajectory in space and time is determined by the optical wave phase profile $\varphi(\mathbf{r}_\perp, z; t)$ through the solution of the system, Eqs. (6a) and (6b), and indicates the direction of optical power flux (the vector $\mathbf{s}_\perp$) along the pulse propagation distance. In general, the local slope of a DR at each point is calculated at different time instants $\tau_{\rm dis}$, which change in accordance with the frequency sweep (pulse self-phase modulation) caused by the pulse GVD process.

Using Eq. (5) one can also write the DR equation in terms of the effective medium permeability $\bar{\varepsilon}_{\rm ef}$:

$$\frac{d^2\mathbf{R}_d}{dz^2} = \frac{1}{2}\nabla_\perp\bar{\varepsilon}_{\rm ef}(\mathbf{R}_d, z; \tau_{\rm dis}). \tag{6c}$$

This is the central equation of the diffraction-ray optics because it establishes a link with the classical geometrical-ray tracing in a medium with some material permittivity $\varepsilon_{\rm ef}$. Equation (6c) indicates that a DR acquires negative angular divergence and bends toward the optical axis when the effective permittivity gradient is negative, $\nabla_\perp\varepsilon_{\rm ef} < 0$, and vice versa if $\nabla_\perp\varepsilon_{\rm ef} > 0$. Consequently, the regions of the medium with negative effective permittivity gradient can be considered as the focusing zones for corresponding DRs, and the regions where $\nabla_\perp\varepsilon_{\rm ef} > 0$ can be treated as the defocusing zones.

Thus, the diffraction beams behave like classical geometrically optic rays, i.e., are the subject of Snell's law of refraction in the presence of a dielectric constant gradient in the medium. The difference between geometrical and diffraction rays is that DRs not only are associated with the material quantity ε_0 but also effectively take into account the diffraction, medium nonlinearity, and chromatic dispersion.

Let us recall the equation for the wave phase, Eq. (3b), and now differentiate both its parts with respect to time. Using the systems of ray characteristics analogous to Eq. (5) we obtain the evolution equation of the so-called temporal diffraction ray $\tau_{\rm dis}$:

$$\frac{d\tau_{\rm dis}}{dz} = -k_\omega''\frac{\partial\varphi}{\partial t}(\mathbf{R}_d, z; \tau_{\rm dis}). \tag{7}$$

The equation of motion for this temporal ray is as follows:

$$\frac{d^2\tau_{\rm dis}}{dz^2} = -k_\omega''\frac{k_0}{2}\frac{\partial\bar{\varepsilon}_{\rm ef}}{\partial t}. \tag{8}$$

In a medium without GVD, $k_\omega'' = 0$, temporal DRs represent the rectilinear trajectories in (t, z) coordinates that run parallel to the pulse time axis. If the medium has a chromatic dispersion, the temporal rays become inclined toward the time axis by an angle given by Eq. (7) even at linear pulse propagation. Depending on the sign of the dispersion coefficient k_ω'', the optical pulse blurs ($k_\omega'' > 0$) or focuses in space ($k_\omega'' < 0$).

B. Conservation laws and diffraction-ray tubes

Let us turn to the equation for optical field amplitude, Eq. (3a). After multiplying both sides by the factor $(2A)$ we obtain the equation for the wave intensity, $I = A^2$:

$$\frac{\partial I}{\partial z} = -\frac{1}{k_0}[I\nabla_\perp^2\varphi + (\nabla_\perp\varphi)\cdot(\nabla_\perp I)] + k_\omega''\left(\frac{\partial\varphi}{\partial t}\frac{\partial I}{\partial t} + I\frac{\partial^2\varphi}{\partial t^2}\right) - \alpha_N I. \tag{9}$$

It is clearly seen that on the right-hand side of this equation in square brackets stays the divergence of the transverse Poynting vector $\mathbf{S}_\perp$. Thus, we come to the equation for the intensity of an optical wave in a nonlinear absorbing and dispersive medium:

$$\frac{\partial I}{\partial z} + \mathrm{div}(\mathbf{S}_\perp) = \frac{\partial S_t}{\partial t} - \alpha_N I, \tag{10}$$

where $S_t = k''_\omega I \frac{\partial \varphi}{\partial t}$. This equation indicates that at every point of the optical path $(\mathbf{r}_\perp, z)$ and at every time instant t the sources of the changes of wave intensity are not only medium absorption and energy cross flows to the neighboring spatial regions but also energy exchange between different pulse time slices.

By time integrating Eq. (10) over infinite limits and noting that $\int_{-\infty}^{\infty} (\partial S_t/\partial t)dt = 0$, we obtain the conservation law for light wave fluence $F(\mathbf{r}_\perp, z) = \int I dt$:

$$\frac{\partial F}{\partial z} + \mathrm{div}(\mathbf{S}_F) = -\langle \alpha_N \rangle_t F. \tag{11}$$

Here the integral parameters are introduced that have the physical meanings of the transverse energy flux vector $\mathbf{S}_F = \int \mathbf{S}_\perp dt$ and time-averaged volume absorption, $\langle \alpha_N \rangle_t = (F)^{-1} \int \alpha_N I dt$.

The optical radiation power, $P(z;t) = \int_S I d\mathbf{r}_\perp$, is of considerable interest in the theory of self-focusing because it determines the whole dynamics of pulse filamentation. Avoiding the loss of generality, we obtain the equation for optical power P flowing through some chosen cross-sectional area S in a laser beam assuming cylindrical symmetry of the problem. Consider two important cases: (a) when this area is the cross section of a cylindrical volume with some constant radius r_c deposited along the laser beam axis, $S = \pi r_c^2$, and (b) when S is a cross section of a DRT, i.e., a cylindrical volume bounded by one of the diffraction rays with a variable in z radial coordinate $R_d(\mathbf{r}_\perp, z; t)$. In the latter case, the area S also has a variable value since the boundary of the DRT varies in space-time.

We use Eq. (10) and integrate it along a circular area with constant radius r_c. After that we come to the relation

$$\frac{\partial P_c}{\partial z} + 2\pi \int_0^{r_c} \mathrm{div}(\mathbf{S}_\perp) r dr = 2\pi \int_0^{r_c} \frac{\partial S_t}{\partial t} r dr - \langle \alpha_N \rangle_S P_c. \tag{12}$$

Here, $P_c = 2\pi \int_0^{r_c} I r dr \equiv \int_0^{r_c} I d\mathbf{r}_\perp$ is the power contained in the cylindrical area, and $\langle \alpha_N \rangle_S = (2\pi/P_c) \int_0^{r_c} \alpha_N I r dr$ denotes the absorption coefficient averaged over the cross section S. Applying the divergence theorem to Eq. (12) we obtain the equation for optical power evolution within the cylindrical volume of a constant cross section:

$$\frac{\partial P_c}{\partial z} = -2\pi r_c S_\perp(r_c) + \frac{\partial}{\partial t}\left[\int_0^{r_c} S_t d\mathbf{r}_\perp\right] - \langle \alpha_N \rangle_S P_c. \tag{13}$$

Now consider the diffraction-ray tube. Because its radius varies along z the differentiation in the first term on the left-hand side of Eq. (10) should be carried out along the integration limit also (Leibniz formula). Taking into account Eq. (6a) for an arbitrary cross section of the DRT, we have

$$\frac{\partial}{\partial z}\left[\int_0^{R_d(z)} I(z) r dr\right] = \left(\frac{dR_d}{dz}\right) R_d I(R_d) + \int_0^{R_d(z)} \frac{\partial I}{\partial z} r dr = S_\perp R_d + \frac{\partial P}{\partial z}. \tag{14}$$

Substituting this relation into the integrated Eq. (10), we obtain the conservation law for the power P_d in a DRT:

$$\frac{\partial P_d}{\partial z} = \int_0^{R_d(z,t)} \frac{\partial}{\partial t} S_t d\mathbf{r}_\perp - \langle \alpha_N \rangle_S P_d, \tag{15}$$

where the absorption coefficient averaging is performed over the DRT section.

As seen, in contrast to a cylinder of constant cross section, Eq. (15) does not contain any light energy fluxes through the lateral ray tube surface (no term with $S_\perp$). In other words, neighboring DRTs do not exchange energy and the change in tube power can only occur due to ohmic losses and redistribution of energy within the laser pulse. This means that at several time instants the losses of DRT power due to absorption can be replenished by the energy influx from the preceding temporal layers of the pulse. In this scenario, the dynamic balance between the focusing and defocusing nonlinearities in the light tube can be restored (or set), thereby supporting (or initiating) the filamentation.

It is straightforward to demonstrate that both Eqs. (13) and (15) after integration with respect to time lead to the same form of the conservation law for total energy Q of the light wave in any selected cross section of the medium S:

$$\frac{\partial Q}{\partial z} = -\int_S \int (\alpha_N I) d\mathbf{r}_\perp dt. \tag{16}$$

Recalling the evolutional equation for optical fluence, Eq. (11), we notice that the parameter $\mathbf{S}_F$ actually represents the wave phase gradient averaged over the pulse envelope weighted by optical intensity I: $\mathbf{S}_F = \int I dt \cdot \int I(\nabla_\perp \varphi) dt = F \cdot \langle \nabla_\perp \varphi \rangle_t$. This allows introducing the additional family of DRs in pulse propagation analysis, the *time-averaged* diffraction rays, which represent energy fluxes within the laser beam, rather than within the pulse as the "instantaneous" DRs $\mathbf{R}_d$ do.

Indeed, if we introduce the averaged vectorial coordinate $\mathbf{R}_{dF} = (1/F) \int \mathbf{R}_d(t) I dt$ then similarly to Eq. (6c) we can write the equation for the averaged (per pulse) diffraction ray:

$$\frac{d^2 \mathbf{R}_{dF}}{dz^2} = \frac{1}{2} \langle \nabla_\perp \bar{\varepsilon}_{\mathrm{ef}} \rangle_t, \tag{17}$$

where $\langle \nabla_\perp \bar{\varepsilon}_{\mathrm{ef}} \rangle_t = \frac{1}{\varepsilon_0 F} \int \nabla_\perp (\varepsilon_N + \varepsilon_d + \varepsilon_{\mathrm{dis}}) I dt$. Thus, the averaged DRs are related not to the intensity of the optical wave but to its energy (fluence) and visualize the direction of the energy flow represented as a change in the coordinate $\mathbf{R}_{dF}$ of such "energy" diffraction ray.

III. EXAMPLES OF DIFFRACTION-RAY PICTURES IN LASER-PULSE FILAMENTATION

In this section we consider several examples of DR tracing that visualize the classical case of Gaussian femtosecond pulse filamentation in air. Worth noting, the diffraction-ray equations Eqs. (6)–(9) provide the complete description of

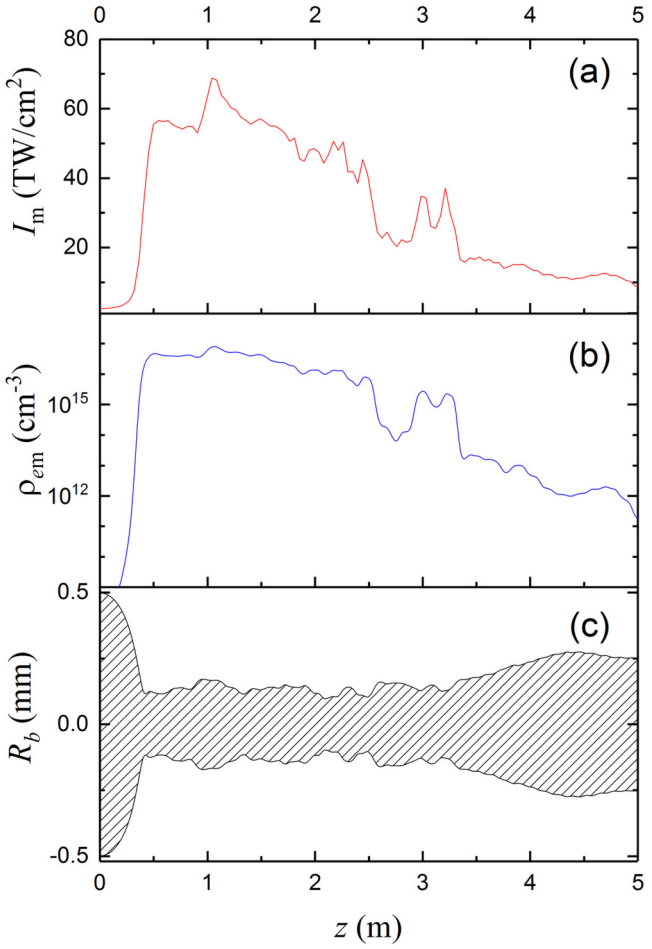

FIG. 1. (a) Peak pulse intensity, (b) density of laser plasma, and (c) beam radius upon laser-pulse filamentation in air.

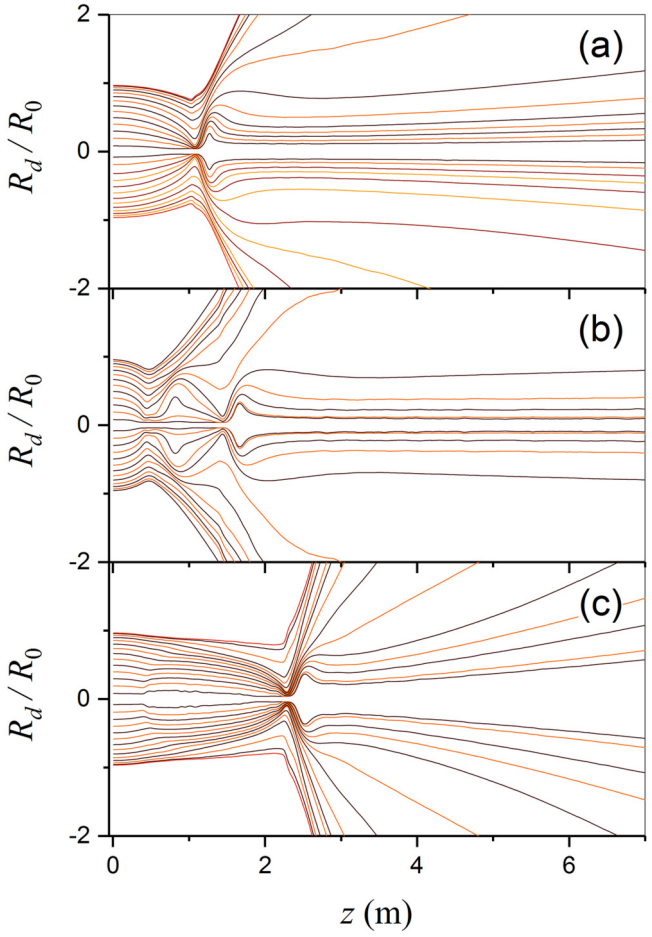

FIG. 2. Trajectories of "instantaneous" DRs R_d for different pulse time slices: (a) $\tau = -1$, (b) 0, and (c) $+1$.

laser-pulse filamentation analogously to the governing paraxial wave propagation Eq. (1). This means that the diffraction-ray formalism is also quantitative, and in principle the ray equations could be solved numerically. However, the numerical solution to the ray equations seems to be more complicated than the well-documented practices of the numerical simulations of Eq. (1). Therefore, to draw ray pictures we numerically solve the original pulse propagation equation Eq. (1) for the electric-field envelope $E(\mathbf{r}_\perp, z\,; t)$ by the spectral Fourier method [1] and obtain spatiotemporal optical phase profile $\varphi(\mathbf{r}_\perp, z; t)$ at every grid point on the propagation path. Then, the calculated nonlinear phase front is used to produce the phase spatial gradient and time derivative profiles. Finally, the DR coordinates $\mathbf{R}_d$ and $\tau_{\rm dis}$ are advanced through the numerical solution to the ray equations Eqs. (6a) and (6b) applying fourth-order Runge-Kutta method.

In the calculations we accept the following parameters of the laser pulse: carrier wavelength $\lambda_0 = 800$ nm, beam radius (at e^{-1} intensity maximum) $R_0 = 0.5$ mm, pulse duration $t_p = 100$ fs, and peak power $P_0 = 6\,P_{\rm cr}$, where $P_{\rm cr}$ is the critical self-focusing power (in air, we take $P_{\rm cr} = 3.2$ GW [1]). Corresponding results of numerical simulations of pulse filamentation are depicted in Figs. 1(a)–1(c). Here we present the variations along the optical path of pulse peak intensity $I_{\rm m}$, peak free-electron density ρ_{em} in air, and beam radius R_b defined according to the fluence profile $F(\mathbf{r}_\perp)$. As follows from these dependences, the propagation of such radiation in air causes its filamentation accompanied by a sharp intensity increase, reduction in pulse size, and formation of a moderate dense plasma region ($\rho_{em} > 10^{14}$ cm^{-3}) along the beam axis.

Now consider the diffraction-ray representation of laser-pulse filamentation. On the series of graphs in Figs. 2(a)–2(c) are plotted DR trajectories for different pulse time instants $\tau = t/t_p$ starting from the front ($\tau = -1$) and ending with the back ($\tau = +1$) pulse edges. In these figures, each diffraction ray is a connected line in (r, z) coordinates, the tangent to which at every point coincides with the direction of normalized transverse Poynting vector $\mathbf{s}_\perp$, and the normal is the local slope of the wave front.

It follows from the diffraction-ray trajectories that the paths of the DRs for different time instants are also different. The diffraction rays on the pulse leading edge [Fig. 2(a)] are practically unaffected by plasma refraction and demonstrate a classical picture of pulse self-focusing with the formation of single nonlinear focus at the distance $z = 1.03$ m. After that, axial DRs enter the spatial region of the gradual increase in their radial coordinate.

The back pulse edge [Fig. 2(c)], on the other hand, suffers mostly from the defocusing in the self-induced plasma created

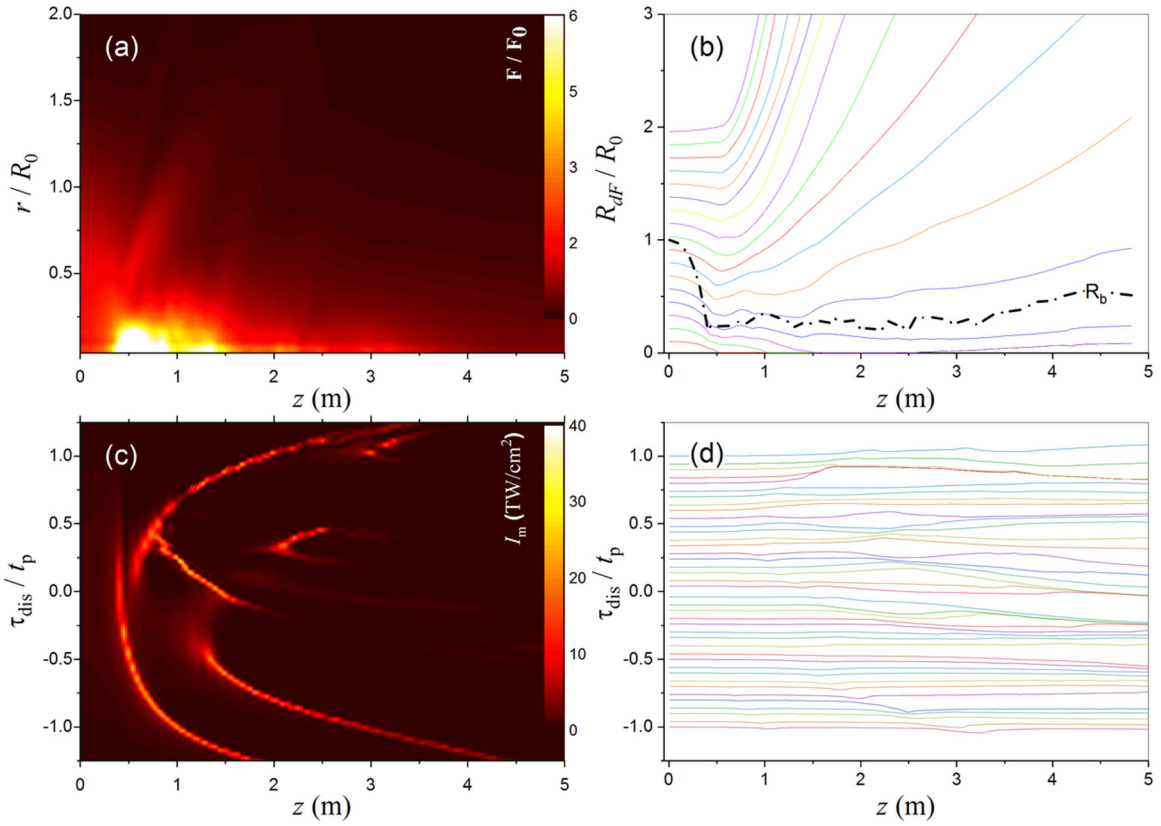

FIG. 3. (a) Pulse fluence profile $F(r, z)$. (b) Time-averaged DR trajectories $R_{dF}(r, z)$. (c) Space-time intensity distribution $I(t, z)$. (d) Temporal DR traces $\tau_{\text{dis}}(t, z)$.

by the previous time slices of the pulse. This leads to a more distant nonlinear focus at $z = 2.2$ m for this time instance. After the nonlinear focus, the corresponding DRs begin to diverge steadily.

Central pulse time layers [Fig. 2(b)] initially contain the major part of radiation power and therefore the first nonlinear focus of this time slice is formed earlier than on the forward edge of the pulse, at $z = 0.54$ m. Some of the peripheral DRs immediately leave the focal region, whereas the paraxial rays demonstrate two more events of nonlinear (re)focusing, the latter of which is observed at $z = 2$ m. From this point the paraxial DRs propagate along the optical axis practically with no divergence.

Worth noting, for the central time layers of the pulse the formation of the so-called diffraction waveguide [27] is well traced on the path section from $z = 0.5$ to 2.2 m. Within this virtual waveguiding channel, the diffraction rays propagate similar to usual geometrical rays in the refractive index-graded waveguide [35]. The condition of medium waveguiding is fulfilled for nonpositive values of the effective dielectric permittivity gradient $\nabla_{\perp}\bar{\varepsilon}_{ef}$ in Eq. (6c). The average diameter of this waveguiding structure is about 300 μm, which is close to the effective size of the spatial region from which the filament consumes light energy according to the concept of the energy reservoir (280 μm as reported in Ref. [36]). In more detail, the energy reservoir in the terminology of DRTs will be considered below.

In Figs. 3(a)–3(d), the "amplitude" and "phase" portraits of the filamentation are presented for comparison. Here, the trajectories of the time-averaged R_{dF} and temporal diffraction rays τ_{dis} are plotted together with the spatial profiles of the pulse fluence and axial intensity. Temporal DR traces are calculated on the beam axis for different moments of local pulse time. Pulse parameters correspond to Fig. 1.

As noted above, a number of closely spaced DRs constitute a diffraction-ray (light) tube, which unlike a single diffraction ray has spatial dimensions and carries a certain amount of pulse power. Ray tubes do not intersect and there is no energy exchange between them. In the approximation of cylindrical symmetry when a single filament is organized on the beam axis, every DR defines its own light tube, the centroid of which coincides with the optical axis, and the boundaries of the tube are determined by the chosen ray trajectory. This leads to a diffraction-ray representation of the propagating laser beam as the evolution of a family of light tubes enclosed into each other.

In contrast to the trajectories of the "instantaneous" diffraction rays in Figs. 2(a)–2(c), the averaged DR traces in Fig. 3(b) demonstrate laser-pulse evolution in a self-induced stationary spatial profile of the effective permittivity gradient $\langle \nabla_{\perp}\varepsilon_{\text{ef}} \rangle_t$. In terms of diffraction-ray optics, laser radiation self-action is expressed as irregular changes in the cross section of averaged DRTs, when some of them are compressed due to self-focusing, while others in contrast increase their sizes and maintain a global divergence of the laser beam.

Diffraction-ray convergence towards the beam axis during pulse self-focusing [first 45 cm of the optical path in Figs. 3(a) and 3(b)] leads to the increase of light tubes numbe and consequently the light energy stored in this region. This, in

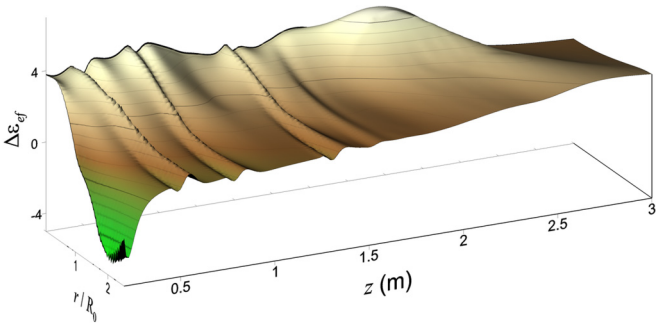

FIG. 4. Effective air permittivity distribution during laser-pulse filamentation.

turn, causes pulse intensity increase, active plasma formation in the medium, and filament formation. In the region where the filamentation exists ($z \sim 3$ m), only slight changes of paraxial DRT area are visible, which indicates the spatial stability of the filament.

As follows from our calculations, the plasma region formed on the beam axis has an average radius of $R_p \sim 30{-}40$ μm, and right in this area all losses of the pulse energy occur. For this reason, light tubes with initial radius $R_d \leqslant R_p$ exhibit the most large-scaled (in percentage) energy losses. In Fig. 3(b) this can be seen as a sharp decrease in the cross section of the first three on-axis DRTs enclosing the filament. Light tubes which are broader (larger boundary radial coordinate) initially carry more radiation energy, and therefore the effect of nonlinear losses due to plasma formation is less noticeable here. As a result, as can be seen in Fig. 3(b), wide tubes with $R_d \gg R_p$ undergo only insignificant compression at the self-focusing stage and practically do not lose energy upon filamentation.

The trajectories of temporal DRs $\tau_{\rm dis}(t, z)$, which show the power flow direction between the different time layers of the laser pulse, are directly connected to the chromatic dispersion of the propagation medium. In the near-IR spectral range, air GVD k''_ω is 0.21 fs^2/cm [1] and therefore the characteristic dispersion length $L_{ds} = t_p^2/k''_\omega$ of a 100-fs pulse considerably exceeds the self-focusing distance. Thus, the temporal diffraction rays shown in Fig. 3(d) run practically parallel to each other up to the nonlinear focus at $z = 0.5$. In this region, plasma production and accompanying this process high nonlinear absorption begin to develop actively. This causes temporal pulse splitting on several shorter subpulses, which are visible on the $I(t, z)$ profile in Fig. 3(c). Simultaneously, this increases the impact of pulse GVD that pushes apart the temporarily short subpulses and broadens the laser pulse as a whole. Temporal DRs at this filamentation stage lose mutual parallelism and some of them demonstrate convergence, thus indicating the emergence of local temporal foci and pulse splitting.

Using the definition of the effective medium permittivity $\varepsilon_{\rm ef}$ it is instructive to establish a direct analogy between the propagation of a beam in a real refractive waveguide and in a virtual self-induced "diffraction" waveguide. Figure 4 shows this entity in the form of time-averaged relative permittivity variation from the initial value along the propagation path: $\Delta\varepsilon_{\rm ef} = (k_0 R_0)^2 \langle \bar{\varepsilon}_{\rm ef} \rangle_t$. The laser-pulse parameters correspond to Fig. 1. Recall that the effective permittivity $\varepsilon_{\rm ef}$ differs from the material permittivity ε_0, which depends only on the physical structure of the medium, by the presence of field contribution accounting for the wave amplitude and phase gradients during pulse propagation.

As can be seen from this figure, the parameter $\Delta\varepsilon_{\rm ef}$ can take positive and negative values during beam propagation, which forms a mountainlike landscape in the effective permittivity profile with characteristic "mountain ridges," "valleys," and "canyons." According to Eq. (6c), the diffraction rays obey the ordinary geometric-ray optics and tend to bend toward larger values of the refractive index. Consequently, meeting an optically dense mountain ridge, a diffraction ray may be captured by these folds and follow its profile until the ray meets an area with higher $\varepsilon_{\rm ef}$ values. When a diffraction ray falls within a canyon, where $\Delta\varepsilon_{\rm ef} < 0$, then it tends to leave this region. If the canyon is not too deep, the ray succeeds in this trend and continues to move toward the positive permittivity gradient ($\nabla_\perp \varepsilon_{\rm ef}$). Otherwise, the canyon walls do not allow the diffraction ray to escape.

Thus, for example, a diffraction ray emitted from the initial plane $z = 0$ with a radial coordinate at the beam boundary $R_d(z = 0) = R_0$ follows the effective permittivity profile. First it bends toward the axis and then turns in the opposite direction to the beam periphery entering the mountain ridges of the $\Delta\varepsilon_{\rm ef}(r, z)$ surface. These ridges are formed as a result of successive nonlinear refocusings of the pulse in the filamentation region. In this area, the radiation intensity sharply increases, which abruptly increases the plasma generation and leads to the decrease or even the change in sign of the nonlinear component ε_N in the expression for $\varepsilon_{\rm ef}$.

A diffraction ray released closer to the beam axis (with a smaller radial coordinate) is initially already at the top of the $\Delta\varepsilon_{\rm ef}$-surface mountain, where smooth changes in the dielectric constant are characteristic. The trajectory of the paraxial ray will be close to rectilinear with slight oscillations during the passage through the folds of $\Delta\varepsilon_{\rm ef}$ values. One can say that such ray enters the diffraction waveguide and is kept by optically dense "diffraction walls" at a certain range.

The peripheral diffraction rays ($R_d > 1.5R_0$) from the very beginning are in the area of negative $\Delta\varepsilon_{\rm ef}$ values, and thus they immediately diverge from the beam axis (they are defocused). At $z \approx 2.3$ m, the paraxial maximum of $\Delta\varepsilon_{\rm ef}$ disappears and shifts to the beam periphery, which indicates the termination of pulse axial self-channeling and the destabilization of its filamentation.

IV. AVERAGED DESCRIPTION OF THE DIFFRACTION-RAY TUBES

The main advantage of the DRT conception of laser radiation propagation is that the light tubes demarcate and separate light energy fluxes within the beam. Since these energy flows are isolated from each other (DRTs do not intersect), each of them can be treated as a separate sub-beam with its own transverse dimensions and angular divergence. Within each sub-beam, the energy conservation law is satisfied. Therefore, as in the case of conventional beams [37,38], averaged (effective) characteristics can be used to describe the evolution of DRTs also.

For definiteness consider the problem of pulse propagation when the conditions of cylindrical symmetry are satisfied. We

associate every DRT with an effective diffraction ray $\langle R_{\rm ed}\rangle$ (ER), the squared coordinate of which represents the time-averaged second-order moment of light intensity I within the DRT cross section:

$$\left\langle R_{\rm ed}^2\right\rangle = (Q)^{-1}\int_{-\infty}^{\infty}\iint_{\mathbf{R}_d(z;t)}[|\mathbf{r}_\perp|^2 I(\mathbf{r}_\perp,z;t)]d\mathbf{r}_\perp dt \quad (18)$$

where $d\mathbf{r}_\perp = rdrd\theta$ is the unit area, θ is the polar angle, and $Q=\int_{-\infty}^{\infty}\iint_{\mathbf{R}_d} I d\mathbf{r}_\perp dt$ is light energy stored in a DRT that obeys the conservation law Eq. (16). We emphasize that an ER by definition does not coincide with DRT boundaries determined by the corresponding DRs, but rather indicates the dimensions of the spatial region where the energy of the optical field is predominantly concentrated. For $R_d\to\infty$, the effective ray $\langle R_{\rm ed}\rangle = \sqrt{\langle R_{\rm ed}^2\rangle}$ of a light tube corresponds to the classical definition of the round-mean-square radius of the entire beam.

For the derivation of the evolutionary equation for $\langle R_{\rm ed}^2\rangle$ we differentiate Eq. (18) with respect to z and take into account the identity

$$\frac{d}{dz}\left(\left\langle R_{\rm ed}^2\right\rangle Q\right) = \int_{-\infty}^{\infty}\iint_{R_d}\frac{d}{dz}(r_\perp^2 I)d\mathbf{r}_\perp dt + \int_{-\infty}^{\infty}\left[R_d^2 I(R_d)\frac{d\mathbf{R}_d}{dz}\right]dt. \quad (19)$$

The integrand in the first term on the right-hand side of this expression can be expanded with the use of Eqs. (6a) and (8):

$$\frac{d}{dz}(r_\perp^2 I) = r_\perp^2\left(-\mathrm{div}(I\mathbf{s}_\perp)+\frac{\partial S_t}{\partial t}-\alpha_N I\right). \quad (20)$$

Applying the divergence theorem and energy conservation law, Eq. (12), we obtain

$$\frac{d\left\langle R_{\rm ed}^2\right\rangle}{dz} = \frac{2}{k_0}\langle|\nabla_\perp\varphi|\mathbf{r}_\perp\rangle - \left[\langle\alpha_N r_\perp^2\rangle - \langle\alpha_N\rangle\left\langle R_{\rm ed}^2\right\rangle\right], \quad (21)$$

where some averaged on time and light tube cross-section parameters are introduced: (a) the mean phase gradient

$$\langle|\nabla_\perp\varphi|\mathbf{r}_\perp\rangle = (Q)^{-1}\int_{-\infty}^{\infty}\iint_{\mathbf{R}_d}((\nabla_\perp\varphi\cdot\mathbf{r}_\perp)\,I)d\mathbf{r}_\perp dt \quad (22a)$$

(b) the mean absorption length

$$\langle\alpha_N r_\perp^2\rangle = (Q)^{-1}\int_{-\infty}^{\infty}\iint_{\mathbf{R}_d}(\alpha_N r_\perp^2 I)d\mathbf{r}_\perp dt \quad (22b)$$

and (c) the mean absorption coefficient

$$\langle\alpha_N\rangle = (Q)^{-1}\int_{-\infty}^{\infty}\iint_{\mathbf{R}_d}(\alpha_N I)d\mathbf{r}_\perp dt. \quad (22c)$$

Comparing Eq. (21) with Eq. (6c) we see that in contrast to the ordinary diffraction ray the equation for the effective ray takes into account the energy absorption in a light tube.

Notice that if we use the non-normalized ray parameter $(\langle R_{\rm ed}^2\rangle Q)$ then the governing ray equation will have a more conventional form:

$$\frac{d\left(\left\langle R_{\rm ed}^2\right\rangle Q\right)}{dz} = Q\left[\frac{2}{k_0}\langle|\nabla_\perp\varphi|\mathbf{r}_\perp\rangle - \langle\alpha_N r_\perp^2\rangle\right]. \quad (23)$$

It is worth deriving the equation for an ER expressed in terms of the effective permittivity $\varepsilon_{\rm ef}$ as in the case of a conventional diffraction ray [see Eq. (6c)]. To this end, we first derive the equation for the transverse Poynting vector component $\mathbf{S}_\perp = \mathbf{s}_\perp I$ and formally write the derivative of this vector along the evolutional coordinate z:

$$\frac{\partial(\mathbf{s}_\perp I)}{\partial z} = I\frac{\partial\mathbf{s}_\perp}{\partial z}+\mathbf{s}_\perp\frac{\partial I}{\partial z} = -\mathbf{s}_\perp I\,\mathrm{div}(\mathbf{s}_\perp)+k_\omega''\frac{\partial\varphi}{\partial t}\frac{\partial(\mathbf{s}_\perp I)}{\partial t} + \frac{1}{2}I\cdot\nabla_\perp\tilde{\varepsilon}_{\rm ef}-\mathbf{s}_\perp\mathrm{div}(\mathbf{s}_\perp I)+\mathbf{s}_\perp\frac{\partial S_t}{\partial t}-\mathbf{s}_\perp I\alpha_N. \quad (24)$$

Applying the vectorial identity, $\mathbf{s}_\perp\mathrm{div}(\mathbf{s}_\perp I)+(\mathbf{s}_\perp I)\mathrm{div}(\mathbf{s}_\perp) = \nabla_\perp[(\mathbf{s}_\perp I)\cdot\mathbf{s}_\perp]$, one obtains the desired equation:

$$\frac{\partial\mathbf{S}_\perp}{\partial z}+\frac{1}{k_0}\nabla_\perp[\mathbf{S}_\perp(\nabla_\perp\varphi)]-\frac{\partial}{\partial t}\left(k_\omega''\frac{\partial\varphi}{\partial t}\mathbf{S}_\perp\right) = \frac{I}{2}\nabla_\perp\bar{\varepsilon}_{\rm ef}-\alpha_N\mathbf{S}_\perp. \quad (25)$$

Then, we scalar multiply Eq. (25) by the coordinate vector $\mathbf{r}_\perp$ and do the temporal and spatial averaging as defined in Eq. (18). As a result, after simple but rather cumbersome mathematics, we get

$$\frac{d\langle\mathbf{s}_\perp\cdot\mathbf{r}_\perp\rangle}{dz} = \frac{1}{2}\langle\nabla_\perp\bar{\varepsilon}_{\rm ef}\cdot\mathbf{r}_\perp\rangle - [\langle\alpha_N\mathbf{s}_\perp\cdot\mathbf{r}_\perp\rangle - \langle\alpha_N\rangle\langle\mathbf{s}_\perp\cdot\mathbf{r}_\perp\rangle]. \quad (26)$$

Here, (a) the mean phase gradient

$$\langle\mathbf{s}_\perp\cdot\mathbf{r}_\perp\rangle = (Q)^{-1}\int_{-\infty}^{\infty}\iint_{\mathbf{R}_d}((\mathbf{s}_\perp\cdot\mathbf{r}_\perp)I)d\mathbf{r}_\perp dt \quad (26a)$$

(b) the mean effective permittivity gradient

$$\langle\nabla_\perp\bar{\varepsilon}_{\rm ef}\cdot\mathbf{r}_\perp\rangle = (Q)^{-1}\int_{-\infty}^{\infty}\iint_{\mathbf{R}_d}((\nabla_\perp\bar{\varepsilon}_{\rm ef}\cdot\mathbf{r}_\perp)I)d\mathbf{r}_\perp dt \quad (26b)$$

And (c) the mean absorption along phase gradient

$$\langle\alpha_N\mathbf{s}_\perp\cdot\mathbf{r}_\perp\rangle = (Q)^{-1}\int_{-\infty}^{\infty}\iint_{\mathbf{R}_d}(\alpha_N(\mathbf{s}_\perp\cdot\mathbf{r}_\perp)I)d\mathbf{r}_\perp dt. \quad (26c)$$

Finally, we take the derivative of Eq. (21) with respect to z, and after substitution of Eq. (26) follows the equation for the squared effective ray of a light tube:

$$\frac{d^2\left\langle R_{\rm ed}^2\right\rangle}{dz^2} = \langle\nabla_\perp\bar{\varepsilon}_{\rm ef}\cdot\mathbf{r}_\perp\rangle - 2[\langle\alpha_N\mathbf{s}_\perp\cdot\mathbf{r}_\perp\rangle - \langle\alpha_N\rangle\langle\mathbf{s}_\perp\cdot\mathbf{r}_\perp\rangle] - \frac{d}{dz}\left[\left\langle\alpha_N r_\perp^2\right\rangle - \langle\alpha_N\rangle\left\langle R_{\rm ed}^2\right\rangle\right]. \quad (27)$$

Obviously, if $\alpha_N\neq\alpha_N(\mathbf{r}_\perp;t)$, e.g., as in a homogeneous linear medium, Eq. (27) formally is identical to the averaged DR

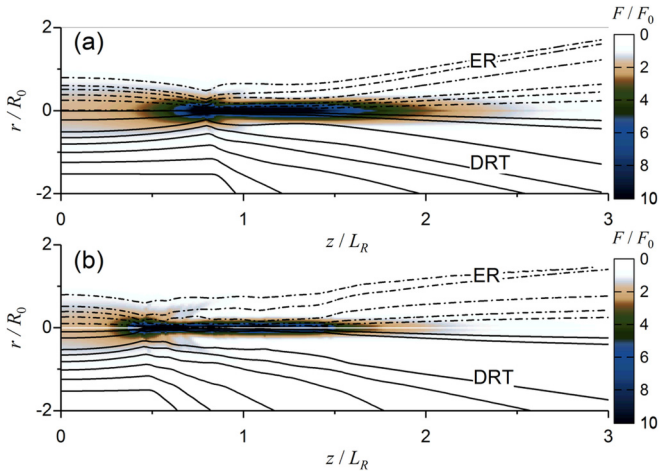

FIG. 5. DRTs (solid lines) and ERs (dash-dotted line) for Gaussian pulse filamentation with (a) $\eta = 3$ and (b) 6.

equation:

$$\frac{d^2\langle R_{\rm ed}^2\rangle}{dz^2} = \langle \nabla_\perp \tilde{\varepsilon}_{\rm ef} \cdot \mathbf{r}_\perp \rangle. \tag{28}$$

In Figs. 5(a) and 5(b), the boundaries of the diffraction-ray tubes and the trajectory of the effective rays of the tubes are plotted for the case of filamentation in air of a Gaussian beam ($R_0 = 2$ mm, $t_p = 100$ fs) with different reduced power $\eta = P_0/P_c$. Here, as a tonal image, the normalized fluence profile $F(r, z)/F_0$ is shown also. DRTs are plotted at the bottom of each figure, and ERs are at the top.

It is clear that due to the initial unimodality of transverse intensity distribution the effective ray of each light tube is located closer to the axis than the corresponding tube boundary. Effective rays completely reproduce all stages of pulse filamentation in terms of energy fluxes dynamics. One can distinguish (a) beam transverse collapsing during its self-focusing, (b) self-channeling of light energy along the axis within the filamentation region, and (c) diffraction broadening of the beam dimensions at the postfilamentation stage.

V. PRACTICAL APPLICATIONS OF DIFFRACTION-RAY OPTICS IN THE FILAMENTATION DYNAMICS

In this section we show how the methodology of diffraction rays and light tubes can be applied in studying laser radiation filamentation dynamics. First we consider the simplified case of steady-state radiation propagation in a nonabsorbing medium with purely Kerr-type nonlinearity (without a plasma and GVD): $\varepsilon_N = 2n_0 n_2 A^2 \equiv \varepsilon_K$, where $I \equiv A^2$ is adopted. In this situation the normalized effective medium permittivity includes only nonlinear and diffraction terms:

$$\tilde{\varepsilon}_{\rm ef} = \frac{2n_0 n_2 A^2}{\varepsilon_0} + \frac{\nabla_\perp^2 A}{k_0^2 A}. \tag{29}$$

As above, we assume cylindrical symmetry of the problem with $\nabla_\perp f(r) \equiv \frac{\mathbf{e}_r}{r}\frac{\partial}{\partial r}(rf)$.

A. Self-channeling conditions of laser radiation

First, we take the Gaussian beam and suppose it retains its profile during the propagation:

$$A(r, z) = A_0(z)\exp[-r^2/2R^2(z)], \tag{30}$$

where A_0 and R are peak amplitude and beam radius, respectively. This approximation is true for quasilinear propagation of a low-power laser radiation ($\varepsilon_K \ll \varepsilon_d$), or, e.g., for the initial stages of self-focusing of radiation with supercritical power, when the self-induced aberrations of the intensity profile are insignificant still.

After substituting Eqs. (29) and (30) into Eq. (26b) we obtain the expression for the mean effective permittivity gradient:

$$\langle |\nabla_\perp \tilde{\varepsilon}_{\rm ef}|\mathbf{r}_\perp\rangle \propto \{\sqrt{2}\big[1 - e^{-\bar{R}_d^2}\big(1 + \bar{R}_d^2\big)\big] - \eta n_0\big[1 - e^{-2\bar{R}_d^2}\big(1 + 2\bar{R}_d^2\big)\big]\}. \tag{31}$$

Here, $\bar{R}_d = R_d/R$, $\eta = \frac{1}{2}(n_2 A_0^2 R^2 k_0^2) \equiv P_0/P_{\rm cr}$ denotes the reduced laser power, $P_0 = A_0^2 \pi R^2$ is initial power, and $P_{\rm cr} = 2\pi/(k_0^2 n_2)$ stands for critical self-focusing power.

The situation when the right-hand side in Eq. (31) is less than or equal to zero is of special interest because this indicates the tendency of radiation channeling in a selected light tube along the propagation path. In this case, the light beam as a whole can stably diverge or converge with respect to the axis, i.e., the effective radius of the entire beam can have a nonzero derivative with respect to z. However, the angular divergence of a given light tube, $\gamma_d \sim d\langle R_{\rm ed}\rangle/dz$, will not increase (as, e.g., during beam diffraction in a linear medium).

Thus, the channeling condition for an ER and, consequently, for the light field in the corresponding DRT is the negative value of the expression in square brackets on the right-hand side of Eq. (31). For two limiting asymptotics, of the paraxial ray ($R_d \ll R$) and the whole beam ($R_d \to \infty$), we obtain the threshold values η^* of relative laser power: $\eta^* = \sqrt{2}/4$ and $\eta^* = \sqrt{2}$, respectively (for $n_0 = 1$). In other words, to trigger the light self-channeling near the beam axis, the initial beam power should be greater than approximately one-third the critical power; in order to suppress beam diffraction as a whole (in terms of the effective radius) about 1.5 times the critical power is required. Notice that the threshold values obtained above refer to the self-channeling of light tubes (virtual sub-beams) and may differ from the threshold power for a stationary aberration-free self-focusing of a Gaussian beam, which is $\eta^* = 1$ as reported in Ref. [39]. The factor $\sqrt{2}$ for the self-channeling threshold of the most outer DR appears as a result of Gaussian profile averaging in the integral relation, Eq. (26b).

Now, consider another important light beam transverse profile in the form of the Bessel-Gaussian (BG) function:

$$A(r, z) = A_0(z)J_0(r/R_B)\exp(-r^2/R^2), \tag{32}$$

where R_B is the central lobe radius and $J_0(r)$ is the zeroth-order cylindrical Bessel function. A similar beam profile is characteristic for the late stages of laser-pulse filamentation, when the so-called plasma-free propagation of the beam is realized and a high-intensity weakly divergent (postfilamentation) light channel is formed along the axis [40].

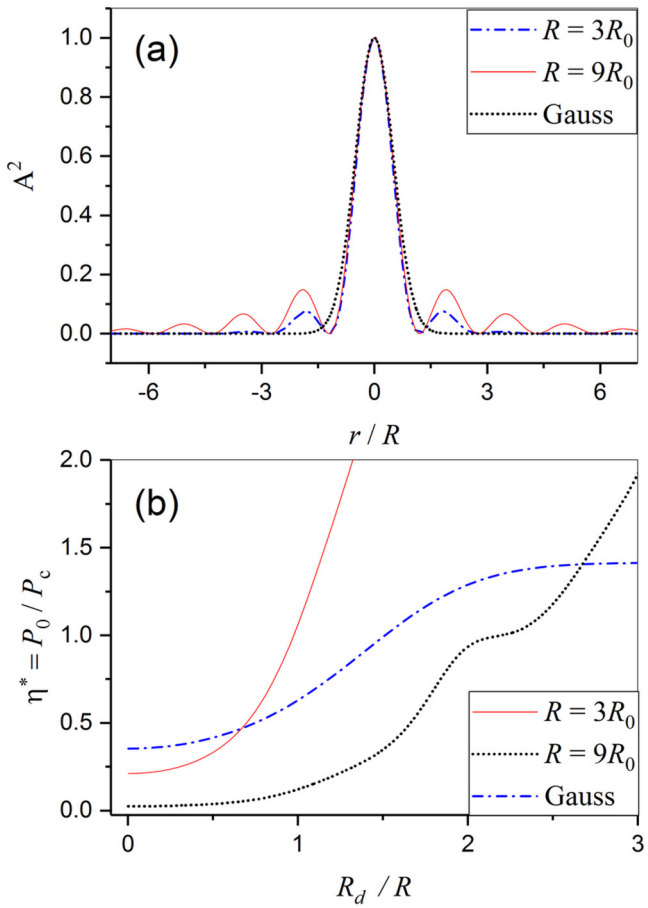

FIG. 6. (a) Transverse intensity profile of Bessel-Gaussian and Gaussian beams. (b) Threshold power for light tube self-channeling as a function of tube radius.

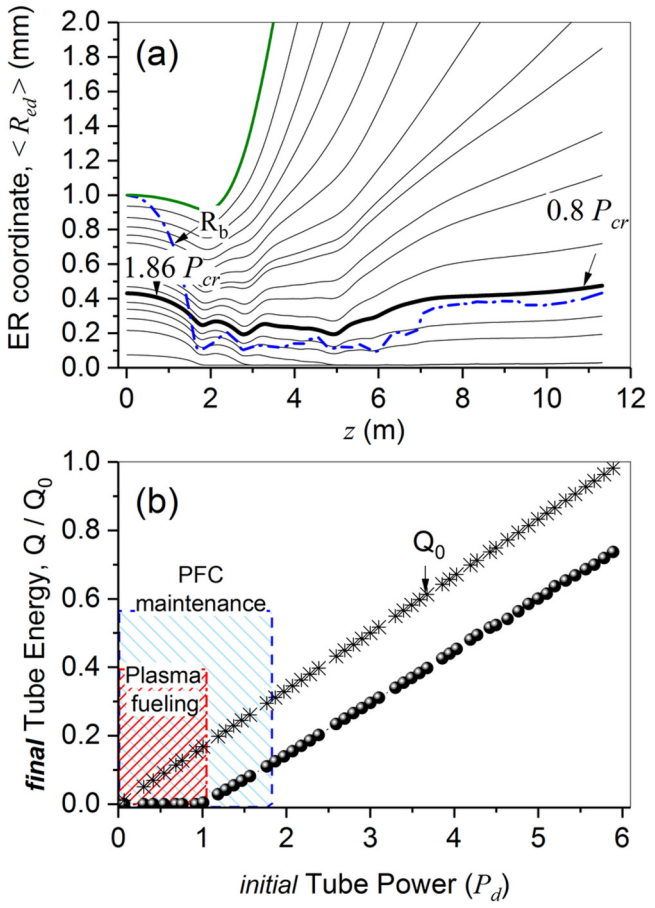

FIG. 7. (a) Effective rays of light tubes during pulse filamentation with $\eta = 6$. (b) Normalized tube energy ($z = 11$ m).

Figure 6(a) shows the intensity distribution of two BG beams with the parameters $R_B = R_0/2$, $R = 3R_0$, and $R = 9R_0$ ($R_0 = 1$ is the radius of a reference Gaussian beam), while in Fig. 6(b) the threshold power of self-channeling of beams is depicted as a function of the light tube radius R_d. These dependences are obtained through the numerical integration of the expression for $\langle \nabla_\perp \bar{\varepsilon}_{\text{ef}} \cdot \mathbf{r}_\perp \rangle$ [Eq. (26b)] after substituting into it the amplitude profile, Eq. (32).

As follows from the presented dependences, the self-channeling threshold for the central part of the BG beam is substantially lower than for the Gaussian profile. At the same time, with an increase in the contrast of the lateral intensity maxima, the threshold values η^* decrease. For a near pure Bessel profile ($R = 9R_0$), the center of the beam propagates in diffraction-free mode at $\eta^* > 0.3$. This indicates that in the case of a BG beam the self-channeling of its central part can be performed at a substantially subcritical power.

The main reason for this behavior is the presence of the ring system in a BG beam encircling the central lobe. As shown [27], each ring represents a specific light diffraction waveguide, which is self-organized around the beam axis during its (non)linear propagation. Within the diffraction waveguide, the radiation propagates with a reduced (relative to diffraction-limited value) angular divergence as evidenced by the lower values of the diffractive permittivity component ε_d calculated for the BG beam (not shown).

B. Postfilamentation light channel

The rather simplified analysis presented above for the conditions of postfilamentation light channeling is confirmed by the numerical calculations of the complete set of propagation equations, Eqs. (1) and (2). Consider Fig. 7(a), which shows the light tube family corresponding to the filamentation of pulsed radiation with the parameters $R_0 = 1$ mm, $t_p = 100$ fs, and $\eta = 6$. Under these conditions, the filamentation region starts approximately at $z = 2$ m and occupies about 4.5 m. Laser beam radius R_b determined from fluence profile $F(r)$ is depicted by the dot-dashed line.

It can be seen that in the filamentation area a waveguiding channel is formed near the optical axis where the light tubes (effective rays) on average retain their sizes. This specific structure contains the filament and the accompanying plasma column. The average size of this structure varies in the range from 100 to 200 μm. After the termination of filamentation at $z \approx 6.6$ m, at the stage of plasma-free propagation the laser beam increases its size and the central (most intense) part forms a postfilamentation channel with a reduced angular divergence.

From the viewpoint of diffraction-ray optics, on the post-filamentation evolutional stage all light tubes demonstrate a

stable spatial expansion that reflects light beam divergence. In this spatial region it is possible to select at least one light tube, which encompasses the postfilamentation light channel (PFC) and has close linear dimensions and angular divergence with this central beam part. This light tube is shown in Fig. 7(a) with a bold line and serves as the energy reservoir for the PFC maintaining its existence as a localized light structure.

If we trace the boundaries of this specific tube back to the filamentation region, we notice that it also serves as an energy reservoir for the filament. This energy replenishing or *refueling* tube covers the intense part of the beam, and its transverse dimension in the filamentation region varies slightly around the level of 200 μm. This value corresponds well to the average size of the bright luminous points experimentally observed inside the filamented laser beam [41,42].

In Fig. 7(b) the relative energy fraction Q/Q_0 in light tubes that remains to the end of propagation is shown as a function of initial tube power P_d. As seen, some of the paraxial tubes with the power $P_d \leqslant P_{cr}$ almost completely lose their energy in the course of pulse filamentation. This energy is consumed on the replenishment of pulse losses during multiphoton absorption and plasma production in the filament. In contrast, light tubes with $P_d > P_{cr}$ exhibit a linear increase in energy content with size, resembling the dependence $Q_0(P_d)$. This indicates a sharp decrease in nonlinear losses in the peripheral areas of the beam. Recall that in the case of cylindrical symmetry light tubes are nested in each other.

As for the PFC, like the filament it is maintained by a specific energy structure, a refueling light tube. According to our calculations [see Fig. 7(a)], the peak power in the initial section of this refueling tube is about twice the critical power for self-focusing. At the end of the propagation range, the PFC power drops to a subcritical value so this light structure can no longer be confined due to Kerr self-focusing only [43].

VI. CONCLUSIONS

In conclusion, we present detailed theoretical formulations of nonstationary diffraction-ray optics as applied to high-power ultrashort laser-pulse propagation in a nonlinear dissipative medium. Within the framework of this concept, the light energy (power) propagates along specific light structures, the *light tubes*. The trajectories of these light tubes at each point of the optical path follow the streamlines of the transverse Poynting vector component. The boundaries of the light tubes do not intersect in space, and the tubes themselves do not exchange light energy. At the same time, their shape and cross-sectional area can vary during pulse propagation representing all physical processes occurring with the radiation in the medium.

In terms of diffraction-ray optics we come to a physical picture of high-power laser-pulse filamentation, when the filament, as an energy sink, consumes light energy not from the entire beam but only from its specific part, which is a light tube too and carries initial power more than the critical power for pulse self-focusing. In fact, it is this light tube that serves as the energy reservoir of the filament. The role of the rest of the light beam (periphery) in the filamentation is the confining of this refueling (replenishing) light tube within the filament boundaries by organizing a virtual diffraction waveguide. Pulse filamentation terminates as soon as the energy in the refueling tube is exhausted. As can be seen, this concept of filamentation combines the characteristic features of two widely known filamentation models, namely, the dynamic spatial replenishment of filament energy from the beam periphery [17] and self-induced waveguide channeling [12].

ACKNOWLEDGMENT

The authors acknowledge financial support by Russian Scientific Foundation Grant No. 16-17-10128.

[1] *Self-Focusing: Past and Present*, edited by Y. R. Shen, R. W. Boyd, and S. G. Lukishova (Springer, Berlin, 2009).

[2] S. Tzortzakis, B. Prade, M. Franco, and A. Mysyrowicz, Time-evolution of the plasma channel at the trail of a self-guided IR femtosecond laser pulse in air, Opt. Commun. **181**, 123 (2000).

[3] A. Couairon and A. Myzyrowicz, Femtosecond filamentation in transparent media, Phys. Rep. **441**, 47 (2007).

[4] S. V. Chekalin and V. P. Kandidov, From self-focusing light beams to femtosecond laser pulse filamentation, Phys.-Usp. **56**, 123 (2013).

[5] C. B. Schaffer, A. Brodeur, J. F. Garca, and E. Mazur, Micromachining bulk glass by use of femtosecond laser pulses with nanoJoule energy, Opt. Lett. **26**, 93 (2001).

[6] A. A. Ionin, S. I. Kudryashov, S. V. Makarov, A. A. Rudenko, L. V. Seleznev, D. V. Sinitsyn, and V. I. Emel'yanov, Nonlinear optical dynamics during femtosecond laser nanostructuring of a silicon surface, Laser Phys. Lett. **12**, 025902 (2015).

[7] V. P. Kandidov, O. G. Kosareva, I. S. Golubtsov, W. Liu, A. Becker, N. Akozbek, C. M. Bowden, and S. L. Chin, Self-transformation of a powerful femtosecond laser pulse into a white-light laser pulse in bulk optical media (or supercontinuum generation), Appl. Phys. B **77**, 149 (2003).

[8] L. Woste, C. Wedekind, H. Wille, P. Rairoux, B. Stein, S. Nikolov, Ch. Werner, S. Niedermeier, H. Schillinger, and R. Sauerbrey, Femtosecond atmospheric lamp, Laser Optoelektron **29**, 51 (1997).

[9] M. Rodriguez, R. Bourayou, G. Méjean, J. Kasparian, J. Yu, E. Salmon, A. Scholz, B. Stecklum, J. Eislöffel, U. Laux, A. P. Hatzes, R. Sauerbrey, L. Wöste, and J.-P. Wolf, Kilometer-range non-linear propagation of femtosecond laser pulses, Phys. Rev. E **69**, 036607 (2004).

[10] R. Ackermann, G. Méchain, G. Méjean, R. Bourayou, M. Rodriguez, K. Stelmaszczyk, J. Kasparian, J. Yu, E. Salmon, S. Tzortzakis, Y.-B. André, J.-F. Bourrillon, L. Tamin, J.-P. Cascelli, C. Campo, C. Davoise, A. Mysyrowicz, R. Sauerbrey, L. Wöste, and J.-P. Wolf, Influence of negative leader propagation on the triggering and guiding of high voltage discharges by laser filaments, Appl. Phys. B **82**, 561 (2006).

[11] M. Durand, A. Houard, B. Prade, A. Mysyrowicz, A. Durécu, B. Moreau, D. Fleury, O. Vasseur, H. Borchert, K. Diener, R. Schmitt, F. Théberge, M. Chateauneuf, J.-F. Daigle, and J. Dubois, Kilometer range filamentation, Opt. Express **21**, 26836 (2013).

[12] A. Braun, G. Korn, X. Liu, D. Du, J. Squier, and G. Mourou, Self-channeling of high-peak-power femtosecond laser pulses in air, Opt. Lett. **20**, 73 (1995).
[13] E. T. J. Nibbering, P. F. Curley, G. Grillon, B. S. Prade, M. A. Franco, F. Salin, and A. Mysyrowicz, Conical emission from self-guided femtosecond pulses in air, Opt. Lett. **21**, 62 (1996).
[14] V. N. Lugovoi and A. M. Prokhorov, A possible explanation of small-scale self-focusing filaments, JETP Lett. **7**, 117 (1968).
[15] A. Brodeur, C. Y. Chien, F. A. Ilkov, S. L. Chin, O. G. Kosareva, and V. P. Kandidov, Moving focus in the propagation of ultrashort laser pulses in air, Opt. Lett. **22**, 304 (1997).
[16] R. Y. Chiao, E. Garmiere, and C. H. Townes, Self-Trapping of Optical Beams, Phys. Rev. Lett. **13**, 479 (1964).
[17] M. Mlejnek, E. M. Wright, and J. V. Moloney, Dynamic spatial replenishment of femtosecond pulses propagating in air, Opt. Lett. **23**, 382 (1998).
[18] A. Lotti, A. Couairon, D. Faccio, and P. Di Trapani, Energy-flux characterization of conical and space-time coupled wave packets, Phys. Rev. A **81**, 023810 (2010).
[19] T. D. Grow, A. A. Ishaaya, L. T. Vuong, A. L. Gaeta, N. Gavish, and G. Fibich, Collapse dynamics of super-Gaussian beams, Opt. Express **14**, 5468 (2006).
[20] T.-T. Xi, X. Lu, and J. Zhang, Spatiotemporal moving focus of long femtosecond-laser filaments in air, Phys. Rev. E **78**, 055401 (2008).
[21] A. A. Zemlyanov, A. D. Bulygin, and Yu. E. Geints, Diffraction optics of a light filament generated during self-focusing of a femtosecond laser pulse in air, Atmos. Ocean. Opt. **25**, 97 (2012).
[22] A. A. Zemlyanov, A. D. Bulygin, Yu. E. Geints, and O. V. Minina, Dynamics of light structures during filamentation of femtosecond laser pulses in air, Atmos. Ocean. Opt. **29**, 395 (2016).
[23] J. Keller, Geometrical theory of diffraction, J. Opt. Soc. **A52**, 116 (1962).
[24] V. I. Talanov, Self-focusing of wave beams in nonlinear media, JETP Lett. **2**, 138 (1965).
[25] S. G. Rautian, Quasi-ray tubes, Opt. Spectrosc. **87**, 456 (1999).
[26] M. Born and E. Wolf, *Principles of Optics* (Cambridge University, Cambridge, England, 1999).
[27] Yu. E. Geints and A. A. Zemlyanov, Ring-Gaussian laser pulse filamentation in a self-induced diffraction waveguide, J. Opt. **19**, 105502 (2017).
[28] Yu. E. Geints, A. A. Zemlyanov, A. A. Ionin, D. V. Mokrousova, L. V. Seleznev, D. V. Sinitsyn, and E. S. Sunchugasheva, Post-filamentation propagation of high-power laser pulses in air in the regime of narrowly focused light channels, Quantum Electron. **46**, 1009 (2016).
[29] W. Braunbek and G. Laukien, Einzelheiten zur Halbebenen-Beugung, Optik **9**, 174 (1952).
[30] P. Ghose, A. S. Majumdar, S. Guha, and J. Sau, Bohmian trajectories for photons, Phys. Lett. A **290**, 205 (2001).
[31] A. S. Sanz, M. Davidović, M. Božić, and S. Miret-Artés, Understanding interference experiments with polarized light through photon trajectories, Ann. Phys. **325**, 763 (2010).
[32] P. Lazzeretti, Topology of quantum mechanical current density vector fields induced in a molecule by static magnetic perturbations, in *Applications of Topological Methods in Molecular Chemistry* (Springer, New York, 2010).
[33] E. A. Skelton and R. V. Waterhouse, Energy streamlines for a spherical shell scattering plane waves, J. Acoustic Soc. Am. **80**, 1473 (1986).
[34] A. D. Polyanin and V. E. Nazaikinskii, *Handbook of Linear Partial Differential Equations for Engineers and Scientists*, 2nd ed. (Chapman and Hall, London, 2016).
[35] L. M. Brekhovskikh, *Waves in Layered Media* (Academic, New York, 1960).
[36] W. Liu, J.-F. Gravel, F. Theberge, A. Becker, and S. L. Chin, Background reservoir: Its crucial role for long-distance propagation of femtosecond laser pulses in air, Appl. Phys. B **80**, 857 (2005).
[37] A. E. Siegman, Defining and measuring laser beam quality, in *Solid State Lasers: New Developments and Applications* (Plenum, New York, 1994).
[38] Yu. E. Geints and A. A. Zemlyanov, On the focusing limit of high-power femtosecond laser pulse propagation in air, Eur. Phys. J. D **55**, 745 (2009).
[39] G. Fibich and A. Gaeta, Critical power for self-focusing in bulk media and in hollow waveguides, Opt. Lett. **25**, 335 (2000).
[40] Yu. E. Geints, A. A. Ionin, D. V. Mokrousova, L. V. Seleznev, D. V. Sinitsyn, E. S. Sunchugasheva, and A. A. Zemlyanov, High intensive light channels formation in post-filamentation region of ultrashort laser pulses in air, J. Opt. **18**, 095503 (2016).
[41] G. Mechain, A. Couairon, M. Franco, B. Prade, and A. Mysyrowicz, Organizing Multiple Femtosecond Filaments in Air, Phys. Rev. Lett. **93**, 035003 (2004).
[42] D. V. Apeksimov, Yu. E. Geints, A. A. Zemlyanov, A. M. Kabanov, G. G. Matvienko, A. N. Stepanov, N. S. Zakharov, and S. V. Kholod, Propagation of a high-power ultrashort laser pulse along a horizontal atmospheric path, Atmos. Oceanic Opt. **23**, 14 (2010).
[43] G. Méchain, A. Couairon, Y.-B. André, C. D'Amico, M. Franco, B. Prade, S. Tzortzakis, A. Mysyrowicz, and R. Sauerbrey, Long-range self-channeling of infrared laser pulses in air: A new propagation regime without ionization, Appl. Phys. B **79**, 379 (2004).